INTERNATIONAL JOURNAL FOR NUMERICAL METHODS IN FLUIDS
Int. J. Numer. Meth. Fluids 2009; **61**:1363–1387
Published online 13 February 2009 in Wiley InterScience (www.interscience.wiley.com). DOI: 10.1002/fld.2001

Toward accurate hybrid prediction techniques for cavity flow noise applications

W. De Roeck*,†, G. Rubio, M. Baelmans and W. Desmet

Department of Mechanical Engineering, K.U. Leuven, Celestijnenlaan 300 B, B-3001 Leuven, Belgium

SUMMARY

A large variety of hybrid computational aeroacoustics (CAA) approaches exist differing from each other in the way the source region is modeled, in the way the equations are used to compute the propagation of acoustic waves in a non-quiescent medium, and in the way the coupling between source and acoustic propagation regions is made. This paper makes a comparison between some commonly used numerical methods for aeroacoustic applications. The aerodynamically generated tonal noise by a flow over a 2D rectangular cavity is investigated. Two different cavities are studied. In the first cavity ($L/D=4, M=0.5$), the sound field is dominated by the cavity wake mode and its higher harmonics, originating from a periodical vortex shedding at the cavity leading edge. In the second cavity ($L/D=2, M=0.6$), shear-layer modes, due to flow-acoustic interaction phenomena, generate the major components in the noise spectrum. Source domain modeling is carried out using a second-order finite-volume large eddy simulation. Propagation equations, taking into account convection and refraction effects, are solved using high-order finite-difference schemes for the linearized Euler equations and the acoustic perturbation equations. Both schemes are compared with each other for various coupling methods between source region and acoustic region. Conventional acoustic analogies and Kirchhoff methods are rewritten for the various propagation equations and used to obtain near-field acoustic results. The accuracy of the various coupling methods in identifying the noise-generating mechanisms is evaluated. In this way, this paper provides more insight into the practical use of various hybrid CAA techniques to predict the aerodynamically generated sound field by a flow over rectangular cavities. Copyright © 2009 John Wiley & Sons, Ltd.

Received 21 August 2008; Revised 22 December 2008; Accepted 29 December 2008

KEY WORDS: cavity noise; aeroacoustics; LES; LEE; hybrid techniques; flow-acoustic coupling

*Correspondence to: W. De Roeck, Department of Mechanical Engineering, K.U. Leuven, Celestijnenlaan 300 B, B-3001 Leuven, Belgium.
†E-mail: wim.deroeck@mech.kuleuven.be

Contract/grant sponsor: Research Foundation of Flanders; contract/grant number: FWO G.0467.05
Contract/grant sponsor: Institute for the Promotion of Innovation by Science and Technology in Flanders; contract/grant number: SBO-IWT 05.0163

1. INTRODUCTION

Aeroacoustics is an area of research of growing interest and importance over the last decade. In the transportation sector, the interest for this field has emerged during the last few years due to different reasons. In aeronautics, for example, strict noise regulations around airports are forcing aircraft manufacturers to reduce the noise emissions during landing and take-off operations. In automotive industry, customer surveys identify wind noise as a regular complaint.

With the increase in computational power, the direct computation of aerodynamic noise has become feasible for academic cases [1–3]. Such a direct approach solves the compressible Navier–Stokes equations, which describe both the flow field and the aerodynamically generated acoustic field. Owing to the large disparity in energy and length scales between the acoustic variables and the flow variables and since acoustic waves propagate in all directions over large distances, the direct solution of the Navier–Stokes equations (DNS) for computational aeroacoustics (CAA) problems is only possible for a limited number of industrial applications.

Therefore, in order to meet the required design times for industrial applications without overshooting the costs, hybrid methods are proposed. In these methods, the computational domain is decomposed into different regions, such that the flow field (source region) and the acoustic field (acoustic region) can be solved with different equations and numerical techniques. As such, the prediction of the acoustic field at large distances from the aerodynamic sound sources is enabled.

Inside the source region the dynamic motion of a compressible fluid is determined by the Navier–Stokes equations, complemented with proper boundary and initial conditions. Since turbulence is responsible for aerodynamic noise generation, large eddy simulation (LES), where the large turbulent scales are directly resolved and the small scales are modeled, seems to be the most efficient numerical approach for solving the source region [4, 5]. As the noise generation problem involves the use of some, from a computational point of view, highly demanding schemes for solving the flow dynamic equations, it is advantageous to have a computational source domain as compact as possible. In this perspective, to formulate the noise propagation problem (acoustic domain) the linearized Euler equations (LEE) [6] and an irrotational formulation of the LEE, the acoustic perturbation equations (APE) [7], are used. These equations provide a physical model that is valid in a medium with non-uniform mean flow and that takes into account all convection and refraction effects.

There exist a large number of coupling techniques to link the source domain with the acoustic propagation domain. In the present study, two different kinds of coupling strategies are elaborated. A first type of coupling is based on an equivalent aeroacoustic source formulation [8–10]. This source formulation is obtained by rewriting the Navier–Stokes equations in such a way that the left-hand side equals the propagation equations that are used, while the remaining terms in the right-hand side are then treated as equivalent aeroacoustic source terms, which can be obtained from the source domain calculation. It is shown that, for applications where acoustic fluctuations inside the source region are not negligible, special care needs to be taken in these source term formulations. In the second coupling technique [11, 12], the acoustic variables, obtained from the noise generation problem in the source domain, serve as boundary conditions for the acoustic propagation equations, resulting in an acoustic continuation of the source domain calculation.

The aim of this paper is to gain more insight into the accuracy of the different hybrid aeroacoustic noise prediction techniques and their ability to predict different tonal flow noise phenomena. For this goal, the aerodynamic noise generation by a flow over rectangular cavities is considered. The laminar, 2D cavity flow presents some peculiar flow features that make it interesting for

DOI: 10.1002/fld

investigating the different CAA methodologies. This application is a reasonable compromise between physical complexity and computational feasibility and has been extensively studied in the literature. Although the sound field for this type of applications might be considered as 2D under certain circumstances [13], the source region should be calculated with a 3D simulation in order not to neglect the inherent 3D nature of turbulence. Nevertheless, the source calculations in this paper are 2D LES. In this way the largest 2D eddies, which are responsible for the dominant, low-frequency tonal components, can be accurately modeled. Broadband components, on the other hand, are generated by the 3D turbulence and will not be predicted in a precise way. Since the goal of the present paper is to study the accuracy of hybrid CAA simulations with respect to the tonal prediction, a 2D approach is thus motivated.

The validation of both the low Reynolds number 2D unsteady flow simulations and the acoustic radiation pattern is performed by a comparative study with existing reference data, obtained from the literature on 2D numerical simulations of identical cavity configurations. Owing to the low Reynolds number and the fact that a 2D simulation is used, a comparison with experimental data is not possible. Furthermore, it is known that certain flow regimes such as the wake mode oscillations, occurring in certain 2D numerical cavity flow simulations, are very difficult to observe experimentally and are therefore considered to be a numerical artifact. Although these features are rather 'unphysical' for real-life cavity applications, they have some particular properties that make them interesting for the validation of hybrid CAA prediction techniques, as shown further in this paper.

The first part of the paper describes the problem of aerodynamic noise generation caused by a flow over a rectangular cavity. The second part describes the source domain modeling techniques and includes a validation of the aerodynamic results for the different oscillation modes. In the third part, the hybrid methodologies are described and the accuracy and the ability of the different coupling techniques to model flow-acoustic interaction effects are evaluated. The major conclusions are summarized in the final section.

2. OPEN CAVITY FLOW

The phenomenon of aerodynamically generated noise by a flow passing over a rectangular cavity has been studied in numerous investigations in the past and has a broad range of applications. These include, but are not limited to, automotive industry, gas transport systems, aircraft wheel and weapon bays, and aerospace applications. The noise spectrum of cavity noise contains both broadband components, introduced by the turbulence in the shear layer, and tonal components. The latter can be induced by two mechanisms: a wake mode mechanism, due to a periodical vortex shedding at the cavity leading edge, and a shear-layer mode mechanism, due to a feedback coupling between the flow field and the acoustic field.

Rossiter [14] was one of the first researchers who described the feedback mechanism based on shadowgraphic observations on a number of different rectangular cavities. Based on these experimental results, Rossiter derived the following semi-empirical formula for the Strouhal number of this periodic phenomenon:

$$St_L = \frac{fL}{U_\infty} = \frac{m - \varsigma}{M_\infty + 1/\kappa} \tag{1}$$

DOI: 10.1002/fld

with L as the length of the cavity, U_∞ the free-stream velocity, m the mode number, $M_\infty = U_\infty / c_\infty$ the undisturbed free-stream Mach number, $\kappa = U_{\text{conv}} / U_\infty$ the ratio of the convection velocity of the vortices (U_{conv}) to the free-stream velocity, and ς a factor to account for the lag time between the passage of a vortex and the emission of a sound pulse at the trailing edge of the cavity.

This periodic flow pattern (with a period T) in the cavity, characterizing the Rossiter modes, can be described by a four-step procedure:

1. Vortices shed from the leading edge of the cavity are convected downstream along the shear layer until they reach the trailing edge of the cavity. This transport of vortices takes a total time T_{vort}, dependent on the length L of the cavity and the vortex convection velocity κ.
2. At the trailing edge, the vortices interact with the downstream wall of the cavity causing, after a certain lag time T_1, the generation of acoustic waves. A part of these acoustic waves are radiated above the cavity into the acoustic far-field.
3. The other part of the acoustic waves (also referred to as pressure waves) are radiated inside the cavity in the upstream direction until they reach the leading cavity edge. The propagation time T_{ac} of the acoustic waves is dependent on the length L of the cavity and the speed of sound c_0. This time is less influenced by the Mach number since the flow velocity inside the cavity is fairly low.
4. When reaching the upstream wall of the cavity, the pressure waves cause the shedding of a new vortex at the leading edge, with a certain lag time T_2. The pressure waves influence the spacing between the different vortices and thus also determine the frequency of this feedback phenomenon.

It is easily shown that the total period $T = 1/f = T_{\text{vort}} + T_1 + T_{\text{ac}} + T_2$ can be written in the form proposed by Rossiter after some assumptions about the lag times T_1 and T_2. In this way, the interaction between vortical and acoustic disturbances create self-sustained oscillations, responsible for tonal noise generation, as is schematically drawn in Figure 1. This oscillation regime is commonly referred to as the Rossiter or shear-layer mode.

Yet another mode of oscillation has been observed. In incompressible experiments, Gharib and Roshko [15] observed that when the length to depth ratio of the cavity is increased, the flow becomes more violent and unsteady. A big vortex that fills the whole cavity is formed at the leading edge and is ejected out of the cavity at the trailing edge when it is big enough. The flow above the

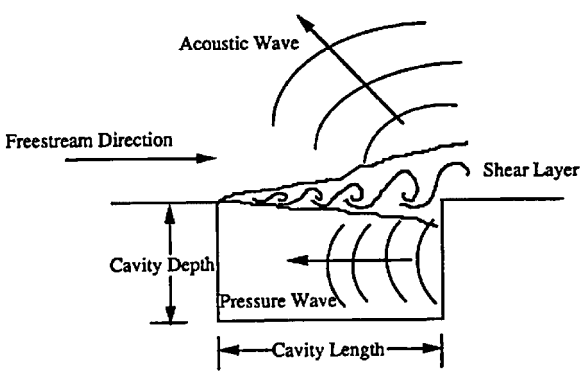

Figure 1. Schematic overview of the shear-layer mode-generating mechanism [13].

DOI: 10.1002/fld

cavity is, in this case, affected by the flow inside the cavity and free-stream fluid is periodically going in and out of the cavity. Gharib and Roshko used the term wake mode to describe this flow regime since the flow over the cavity looks like the wake behind a bluff body. Flow features of this mode are qualitatively very different from shear-layer mode. Numerical studies [1] show that, in wake mode, the frequencies of oscillation are independent of the Mach number, suggesting the absence of a flow-acoustic coupling. It should be mentioned that this oscillation mode is, however, rarely observed in compressible 3D experiments.

Experimental cavity flow research is dominated by the study of near-field flow features and cavity-wall pressure fluctuations. Several reviews of these experimental results are given in the literature [16–19]. From a computational point of view, many studies about cavity flow exist in the literature. Recently, shear-layer and wake modes have been numerically investigated by several authors using 2D direct numerical simulation [1, 2, 20] in the frame of aeroacoustic research. Owing to extended knowledge about the noise-generating mechanisms, the numerical study of 2D cavity noise has become an aeroacoustic benchmark problem that allows one to evaluate the performance of the hybrid CAA techniques for tonal noise generation by both purely aerodynamic and flow-acoustic feedback mechanisms.

2.1. Description of the numerical setup

The two cavities that are considered in this paper were previously computed using DNS by Rowley [1]. In the first cavity, labeled as $4M5$ ($L/D=4$, with D the depth of the cavity and $M=0.5$), the sound field is dominated by the wake mode of the cavity, originating from the periodical vortex shedding at the cavity leading edge, and its higher harmonics. In the second cavity, labeled as $2M6$ ($L/D=2$ and $M=0.6$), shear-layer modes, due to flow-acoustic interaction phenomena, generate the major components in the noise spectrum. The Reynolds number of both computations based on the depth of the cavity Re_D is 1500 and the ratio L/θ_0, where θ_0 is the boundary-layer momentum thickness at the leading edge of the cavity due to the initial conditions, is equal to 102 for the case $4M5$ and to 52.8 for $2M6$.

Figure 2 shows the computational domain for both the source and the propagation region and indicates several system parameters.

With an origin of the coordinate system situated at the leading edge of the cavity, the computational LES domain for the cavity $4M5$ extends from $-4.3\leqslant x/D\leqslant 13.2$ and $-1.0\leqslant y/D\leqslant 3$, whereas for the cavity $2M6$, $-4.3\leqslant x/D\leqslant 9.8$ and $-1.0\leqslant y/D\leqslant 3$. On all solid walls, no-slip and

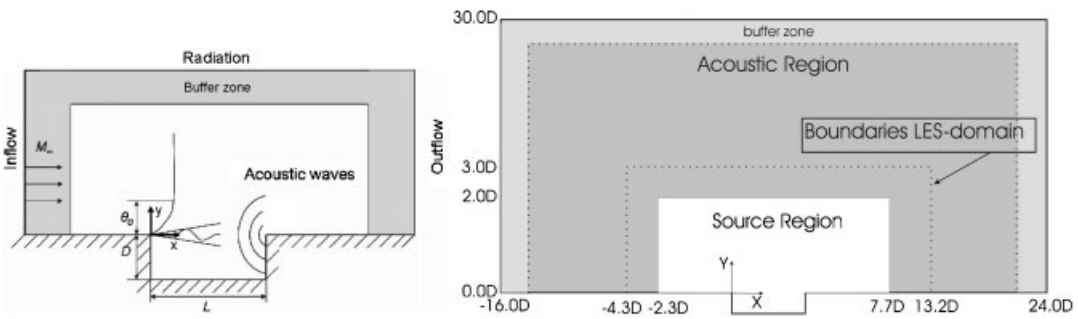

Figure 2. Cavity configuration and computational domain for the cavity $4M5$.

DOI: 10.1002/fld

no-penetration conditions are imposed. The LES mesh is refined toward the walls and in the region of the mixing layer. The mesh is also progressively stretched toward the outlet region to help dissipating vortical structures before they reach the outlet boundary with a maximum stretching of 5%. Owing to the fact that second-order schemes are used for the LES, the mesh size has to be taken small enough to avoid excessive dispersion and dissipation errors that can contaminate the acoustic information. The mesh is approximately of size $\Delta x \approx 8 l_\eta$ (l_η being the Kolmogorov length scale) and $y^+ \leqslant 1$ near the walls. For DNS, the mesh size has to be $\Delta x \leqslant 2 l_\eta$ in the free-shear region; therefore, a Smagorinsky subgrid scale model is used to simulate the effect of the unresolved scales. The total number of cells in the source region is 101 000 for the cavity $4M5$ and 83 000 for the cavity $2M6$. The computations are started from an initial solution consisting of a Blasius flat plate laminar boundary layer spanning the whole domain, including the cavity, and are run until statistically steady state is reached. A Courant-Friedrichs-Levy (CFL) number equal to 3.0 is used, resulting in a non-dimensional timestep of approximately 0.0035.

After the LES simulations, the acoustic calculations are carried out on an equidistant Cartesian mesh, containing approximately 500 000 nodes for both the cavities $4M5$ and $2M6$. The grid size Δx_{ac} is taken equal to $0.05D$ in both directions. The acoustical domain has a total height of $30D$ above the cavity and a length of $40D$, starting at a distance of $16D$ before the cavity leading edge. The computational domain is shown on the right side of Figure 2. The calculations are carried out over 11 000 timesteps with a CFL number equal to 0.75 resulting in a non-dimensional timestep of 0.0375, which is more than 10 times the non-dimensional timestep of the unsteady flow simulation. The results of the last 9000 timesteps are used to obtain results in the frequency domain since approximately 2000 timesteps are needed to obtain a steady-state solution in the propagation region. The source region used for the propagation equation has a height of $2D$ and a length of $10D$, ranging from $-2.3D$ to $7.7D$ in the x-direction. This is slightly smaller than the total domain used to solve the LES in order to minimize the effect of the boundary conditions on the fluctuating variables inside the flow domain. The values at the border of this source region are used when the coupling between the acoustic field and the flow field is elaborated with acoustic boundary conditions.

As shown in Figure 3 the computational grids for the unsteady flow simulations and the acoustic simulations significantly differ from each other. An important issue for hybrid CAA methodologies is the transfer of coupling information between these non-matching grids. The mapping of data from the LES grid onto the acoustic grid must be carried out in such a way that the information contained in the smallest scales of the original source description is not lost. Commonly used linear interpolation schemes do not conserve the original source description and for this reason a conservative mapping technique is used [21].

A mapping scheme is conservative if the integral of the transferred variable g is conserved. g can be the equivalent source term formulation, using acoustic analogies, or the velocity, pressure, and density fluctuations when using acoustic boundary condition as coupling formulation. The following relation then holds between g_j and G_k, being, respectively, the values at the fine LES and coarse acoustic grid, which are both assumed to be constant along the volume v_j, respectively, V_k, of each element:

$$\sum_j g_j v_j = \sum_k G_k V_k \tag{2}$$

For the transfer of surface distributed equivalent sources or acoustic boundary condition values, the same relation holds with the different element volumes replaced by the respective surfaces.

DOI: 10.1002/fld

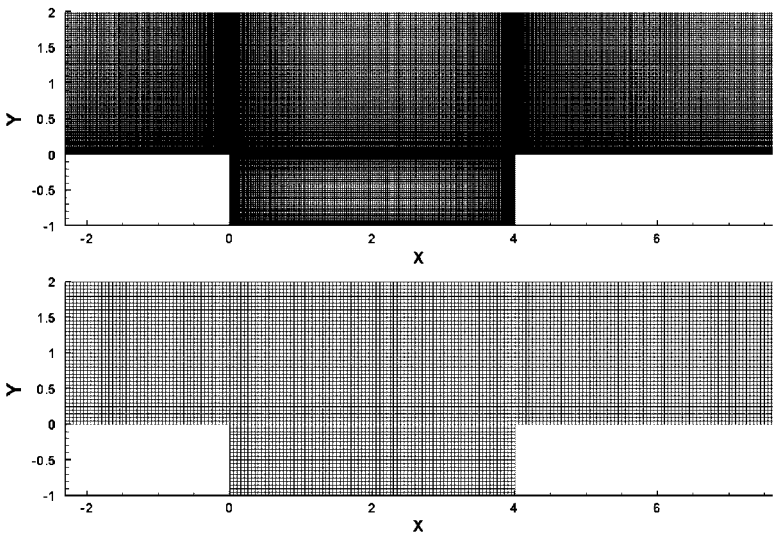

Figure 3. Computational grids used for the interpolation of the equivalent sources of the LES simulation (top) and acoustic simulation (bottom) for the cavity $4M5$.

The relationship between the values that need to be interpolated between the different grids can be expressed as

$$G_k = \sum_j \alpha_{jk} g_j \tag{3}$$

where α_{jk} are the interpolation coefficients, which have to satisfy following relation for the scheme to be conservative:

$$\sum_k \alpha_{jk} = 1 \quad \forall j \tag{4}$$

In this paper, an inverse distance-based interpolation scheme is used:

$$\alpha_{jk} = f(r_{jk}) \Big/ \sum_i f(r_{ji}) \quad \text{with} \begin{cases} f(r_{jk}) = 1/r_{jk} & \text{if } r_{jk} \leqslant r_{\max} \\ f(r_{jk}) = 0 & \text{if } r_{jk} > r_{\max} \end{cases} \tag{5}$$

with r_{jk} as the distance between the gridpoint j of the fine LES grid and the gridpoint k of the coarse acoustic grid. Within a maximum distance of $r_{\max}$ from each gridpoint of the coarse grid, the cells of the fine grid are taken into account for the interpolation routine. This distance is taken to be equal to twice the grid size of the equidistant acoustic grid Δx_{ac}.

3. SOURCE REGION MODELING

3.1. Filtered compressible Navier–Stokes equations

The compressible LES equations for a viscous flow are obtained from a decomposition of the variables of the Navier–Stokes equations (ρ, u_i) into a Favre-filtered part $(\overline{\rho}, \widetilde{u_i})$ and an unresolved

DOI: 10.1002/fld

part (ρ', u_i') that has to be modeled with a subgrid scale model (the detailed expressions for the filters and for the subgrid scale terms can be found, for example, in [22]):

$$\frac{\partial \overline{\rho}}{\partial t}+\frac{\partial \overline{\rho}\widetilde{u}_i}{\partial x_i}=0 \tag{6}$$

$$\frac{\partial \overline{\rho}\widetilde{u}_i}{\partial t}+\frac{\partial \overline{\rho}\widetilde{u}_i\widetilde{u}_j}{\partial x_j}=-\frac{\partial \overline{p}}{\partial x_i}+\frac{\partial(\widetilde{\tau}_{ij}+\tau_{ij,\mathrm{SGS}})}{\partial x_j} \tag{7}$$

$$\frac{\partial \overline{\rho}\widetilde{e}}{\partial t}+\frac{\partial \overline{\rho}\widetilde{e}\widetilde{u}_i}{\partial x_i}=-\frac{\partial \widetilde{u}_i\overline{p}}{\partial x_i}+\frac{\partial \widetilde{u}_i(\widetilde{\tau}_{ij}+\tau_{ij,\mathrm{SGS}})}{\partial x_j}-\frac{\partial(\widetilde{q}_i+q_{i,\mathrm{SGS}})}{\partial x_i} \tag{8}$$

where $\overline{\rho}$, $\widetilde{u}_i$, and $\overline{p}$ are the resolved density and velocity components and pressure. For a perfect gas, the total energy per mass unit $\widetilde{e}$ is defined as $\overline{p}/(\gamma-1)\overline{\rho}+(\widetilde{u}_1^2+\widetilde{u}_i\widetilde{u}_i)/2$ with γ as the ratio of specific heats. The viscous stress tensor $\widetilde{\tau}_{ij}$ is modeled as a Newtonian fluid, and the heat flux $\widetilde{q}_i$ is modeled with Fourier's law. Dynamic molecular viscosity and molecular conductivity are kept constant.

The subgrid scale tensor, $\tau_{ij,\mathrm{SGS}}$, and the subgrid scale heat flux, $q_{i,\mathrm{SGS}}$, reproduce the dissipative effects of the unresolved scales by using a turbulent viscosity μ_t and a turbulent Prandtl number Pr_t, the latter taken to be equal to 0.5 for all calculations. The subgrid scale stress tensor and the subgrid scale heat flux are then modeled as $\tau_{ij,\mathrm{SGS}}=2\mu_t\widetilde{S}_{ij}$ and $q_{i,\mathrm{SGS}}=-(\mu_\mathrm{t}c_p/Pr_\mathrm{t})\partial\widetilde{T}/\partial x_i$, with $\widetilde{T}$ as the temperature and $\widetilde{S}_{ij}=\frac{1}{2}(\partial\widetilde{u}_i/\partial x_j+\partial\widetilde{u}_j/\partial x_i)$.

To determine the turbulent viscosity, a Smagorinsky model is used, where $\mu_\mathrm{t}=\overline{\rho}(C_\mathrm{s}\Delta)^2\sqrt{2\widetilde{S}_{ij}\widetilde{S}_{ij}}$. The Smagorinsky constant C_s is set to 0.1 as suggested by Deardorff [23] for wall bounded flows, and the filter size Δ is locally set to the cube root of the cell volume. To take into account the scale reduction that occurs near walls, the filter size Δ is weighted with the normal wall coordinate y^+ in the way proposed by Van Driest: $\Delta'=\Delta(1-\exp(-y^+/A))$, with $A=25$.

3.2. Numerical implementation

The filtered compressible Navier–Stokes equations are implemented in an in-house finite-volume code. They are integrated in time using a fourth-order explicit Runge–Kutta scheme. Convective and viscous terms are discretized using central second-order schemes. On all solid walls, no-slip and no-penetration conditions are imposed, with $\partial p/\partial n=0$, n being the direction normal to the wall. At the upstream boundary, characteristic soft inflow conditions, proposed by Kim and Lee [24], are applied. At the outlet, the subsonic non-reflecting outflow condition of Poinsot and Lele [25] is implemented. At the top boundary of the domain, radiation boundary conditions of Tam and Dong [26] are used.

To minimize the reflection generated by acoustic waves and vortical structures at the boundaries, a buffer layer [27] has been added to the computational domain. The buffer zone contains 50 cells near the upstream and downstream boundaries and 20 cells near the top (radiation) boundary. In this buffer layer, vortical structures and acoustic waves are dissipated by an additional term included in the right-hand side of Equations (6)–(8):

$$\frac{\partial U}{\partial t}+\cdots=-\frac{\overline{c}}{\Delta x_i}\sigma_{\max}\left(\frac{x_i-x_{i,0}}{x_{i,\max}-x_{i,0}}\right)^{\alpha}(U-U^*) \tag{9}$$

DOI: 10.1002/fld

where $\overline{c}$ is the average speed of sound based on statistical quantities during the computation, $\sigma_{\max}$ is a buffer parameter, $x_{i,0}$ and $x_{i,\max}$ are the coordinates, normal to the boundary, indicating the beginning and the end of the buffer zone, $\alpha=2$, U is the vector of conservative variables, and U^* is the target state for these variables, equal to the free-stream conditions.

4. SOURCE REGION RESULTS

The discussion of the results obtained with the unsteady flow simulations for both cavities is limited to a short description of two different oscillation regimes: the shear-layer mode and the wake mode that are identified for, respectively, the cavities $2M6$ and $4M5$. A more detailed analysis of the source region results including the transition between the two different oscillation regimes and computational issues such as the convergence and stability of the presented results is described in [28, 29].

4.1. Shear-layer mode

The shear-layer mode is characterized by the roll-up of vorticity in the shear layer. The vortices created are then convected with the mean flow until they hit the downstream edge of the cavity. At that moment, acoustic waves are generated that propagate upstream, exciting the shear layer at the upstream cavity edge. Figure 4 shows, for the cavity $2M6$, vorticity contours at four different instants, corresponding, approximately, to $\frac{1}{4}$ phase intervals of the second Rossiter mode, which is dominant for this computation. A steady vortex occupying the rear half of the cavity is identified, evidencing that the interaction of the shear layer with the flow inside the cavity is very weak for this mode of oscillation.

In order to identify the frequencies of oscillation, time signals of the primitive variables have been recorded at different points in the shear layer. The left side of Figure 5 shows the frequency transform of v/U_∞ at a point $(1.6D, 0)$ for the cavity $2M6$ after the flow has been statistically converged. The dominant frequency occurs at an St_D of 0.19. This number is in reasonable agreement with the value of 0.159 predicted by Equation (1) for the first shear-layer mode with $\kappa=0.57$ and $\varsigma=0.25$ as suggested by Rossiter [14]. The shear-layer mode shows mean flow streamlines (right side of Figure 5) nearly horizontal across the mouth of the cavity.

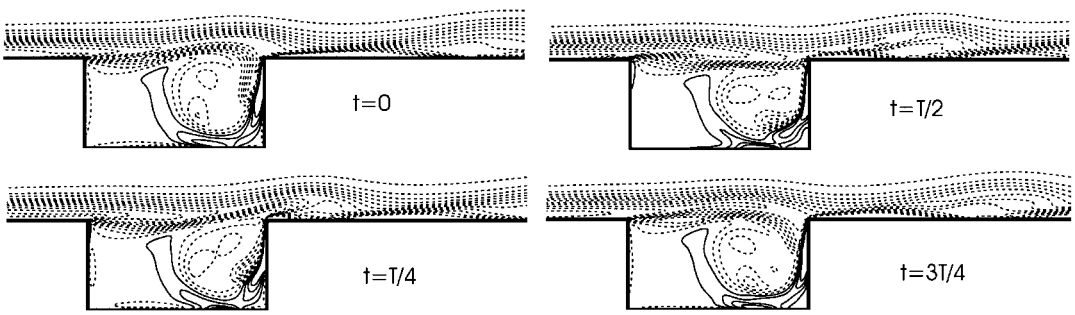

Figure 4. Vorticity field during one cycle of oscillation for the cavity $2M6$ (first Rossiter mode). Fifteen contours of $\omega_z D/U_\infty$ are shown between -5 and 1.67 (negative contours are dashed).

DOI: 10.1002/fld

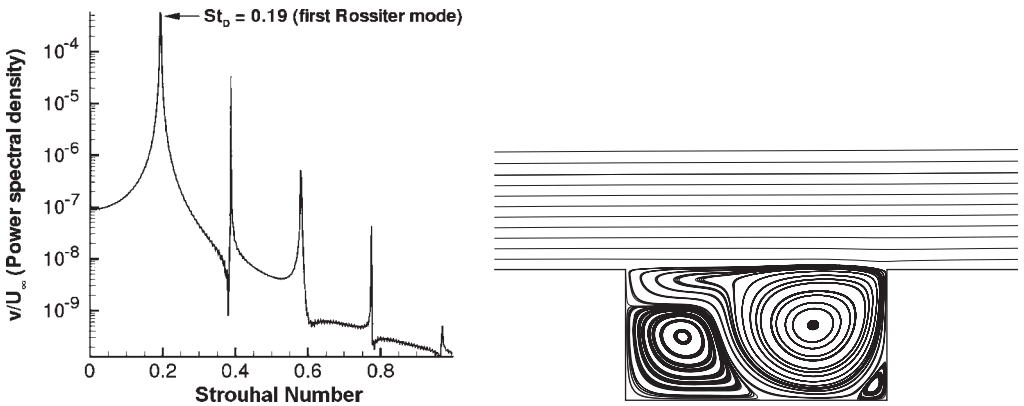

Figure 5. FFT at a position $(1.6D, 0)$ (left) and time-averaged streamlines (right) for the cavity $2M6$ oscillating.

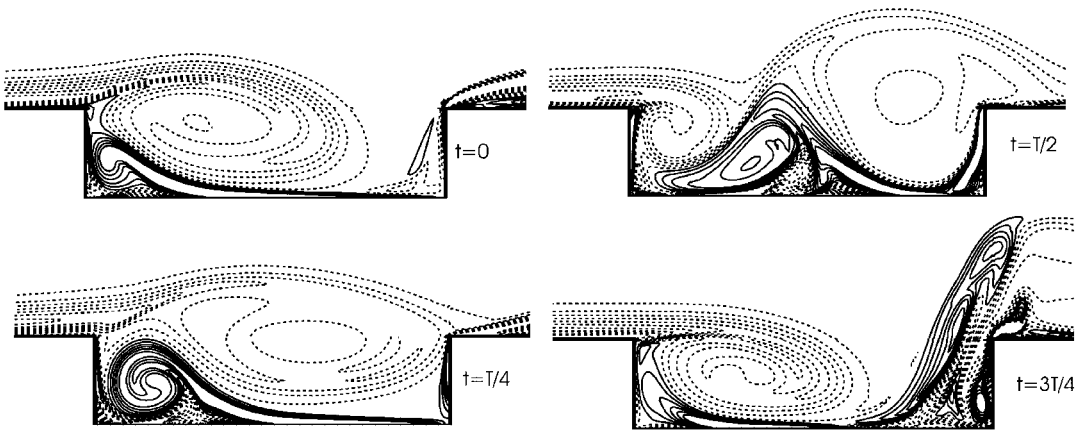

Figure 6. Vorticity field during one cycle of oscillation for the cavity $4M5$. Sixteen contours of $\omega_z D/U_\infty$ are shown between -5 and 3 (negative contours are dashed).

4.2. Wake mode

As the length of the cavity, relative to the momentum thickness of the boundary layer at the leading edge, or the Mach number is increased, there is a substantial change in the pattern of the cavity oscillations [28]. Under these conditions, the flow is characterized by a large-scale vortex shedding from the cavity leading edge. The vortex reaches nearly the cavity size, dragging during this formation irrotational free-stream fluid into the cavity. The vortex is then shed from the leading edge and violently ejected from the cavity. In this case the boundary layer separates upstream during the vortex formation and downstream, as it is convected away. These events are clearly visible for the cavity $4M5$, as shown in Figure 6.

DOI: 10.1002/fld

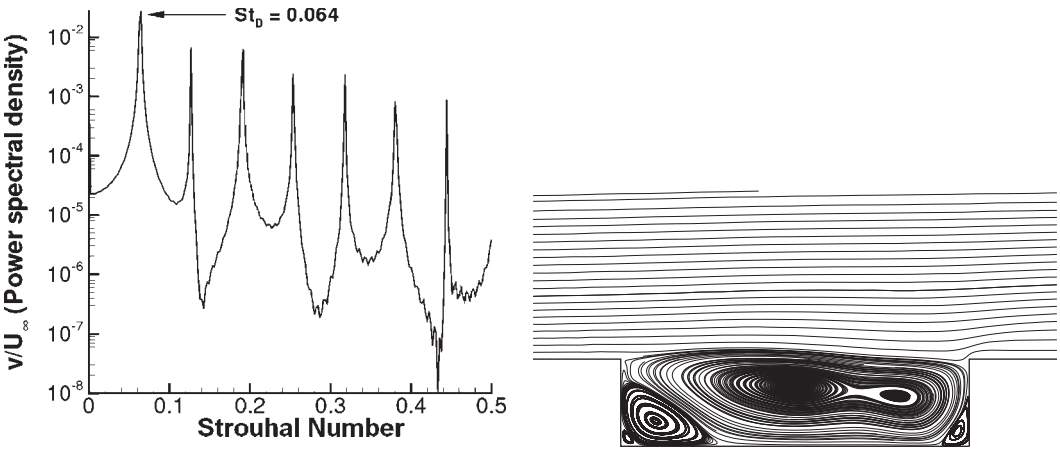

Figure 7. FFT at a position $(3.2D, 0)$ (left) and time-averaged streamlines (right) for the cavity $4M5$ oscillating in the wake mode.

The left side of Figure 7 shows the frequency transform of v/U_∞ at a point $(3.2D, 0)$ located in the shear layer for the cavity $4M5$ after the flow has been statistically converged. The dominant frequency occurs at an St_D of 0.064. This is in agreement with the DNS results of Rowley [1] and is the dominant frequency for cavities oscillating in the wake mode, independent of the Mach number. The streamlines above the cavity, shown on the right side of Figure 7, are clearly deflected in the wake mode. The oscillations in a wake mode have a significant impact on the mean flow outside the cavity. It is important to remark that they affect the pattern of this mean flow even in the upstream direction. Owing to this, the momentum thickness at the leading edge that is imposed as an initial condition is different from the momentum thickness that is found in the statistically converged flow.

From these results it is clear that the noise-generating mechanisms for both cavities strongly differ from each other. The wake mode is generated by purely aerodynamic phenomena, characterized by high-amplitude turbulent velocity fluctuations, and compressible effects can be safely neglected for this oscillation regime. The shear-layer mode, on the other hand, is characterized by low-amplitude velocity fluctuations, resulting in a lower disparity between the aerodynamic and acoustic fluctuating variables and, as a result, compressible effects can no longer be neglected to describe this noise-generating mechanism.

5. ACOUSTIC DOMAIN MODELING

Hybrid CAA computations use the results of the source region as an input to calculate the acoustic near- and far-fields. Hence, the modeling of the acoustic region is strongly influenced by the accuracy of the source region results. Different equations can be used to describe the propagation of acoustic waves in a non-quiescent medium and a number of different coupling techniques are available. This paper mainly focuses on commonly used coupling techniques and uses propagation equations that describe the acoustic near-field and thus take into account mean flow effects as convection and refraction.

DOI: 10.1002/fld

5.1. Propagation effects

LEE are commonly used to describe the near-field propagation of acoustic waves in the presence of a non-uniform mean flow [6]. Opposite to the linear acoustic wave equation (AWE) and the convective wave equation (CWE), the LEE take into account all refraction and convection effects caused by the presence of a non-uniform mean flow field. Acoustic dissipation due to the viscosity of the mean flow field is not taken into account but this effect can be assumed to be negligible for this type of applications. The LEE are obtained by decomposing the flow variables of the Navier–Stokes equations into their mean values (ρ_0, U_0, p_0) and their fluctuating (acoustic) parts (ρ', u', p') and by neglecting viscosity and higher-order terms:

$$\frac{\partial \rho'}{\partial t} + \frac{\partial}{\partial x_i}(\rho_0 u_i' + \rho' U_{i0}) = \Phi_{\text{cont}} \tag{10}$$

$$\frac{\partial}{\partial t}(\rho_0 u_i') + \frac{\partial}{\partial x_j}(\rho_0 u_i' U_{j0}) + \frac{\partial p'}{\partial x_i} + (\rho_0 u_j' + \rho' U_{j0})\frac{\partial U_{i0}}{\partial x_j} = \Phi_{\text{mom},i} \tag{11}$$

$$\frac{\partial p'}{\partial t} + \frac{\partial}{\partial x_i}(\gamma P_0 u_i' + p' U_{i0}) + (\gamma - 1) p' \frac{\partial U_{i0}}{\partial x_i} - (\gamma - 1) u_i' \frac{\partial P_0}{\partial x_i} = \Phi_{\text{ener}} \tag{12}$$

where Φ_{cont}, $\Phi_{\text{mom},i}$, and Φ_{ener} are the acoustic sources for, respectively, the continuity, momentum, and energy equations. They may contain both external applied mass, force and energy sources and aeroacoustic sources, and non-linear and visco-thermal interaction phenomena that can be calculated based on the time-dependent source domain results. These source term formulations are discussed in more detail in the following section. The mean flow variables (ρ_0, U_0, p_0) can be easily obtained by calculating the Reynolds-averaged Navier–Stokes (RANS) equations for the total propagation region.

Although the LEE describe the propagation of acoustic waves in a non-quiescent medium, they also support the propagation of vorticity and entropy waves, which can lead to non-acoustic, unphysical, or even unstable acoustic solutions if the source terms excites the entropy or vorticity modes of the LEE [7]. The presence of entropy and vorticity waves as a solution of the propagation equations can be avoided by assuming that the acoustic field is irrotational ($\vec{\omega'} = 0$) and isentropic ($\mathrm{d}p = c_0^2 \mathrm{d}\rho$ with $c_0 = \sqrt{\gamma P_0/\rho_0}$, the mean speed of sound). Under these assumptions, the LEE can be rewritten as

$$\frac{\partial p'}{\partial t} + c_0^2 \nabla \cdot \left(\rho_0 \mathbf{u}' + \mathbf{U}_0 \frac{p'}{c_0^2} \right) = c_0^2 \Phi_{\text{cont}} \tag{13}$$

$$\frac{\partial \mathbf{u}'}{\partial t} + \nabla(\mathbf{U}_0 \cdot \mathbf{u}') + \nabla\left(\frac{p'}{\rho_0}\right) = \frac{\boldsymbol{\Phi}_{\text{mom}}}{\rho_0} \tag{14}$$

This set of equations is also known as the APE [7] or the linearized perturbed compressible equations [30, 31]. It can be proven that these equations render perfectly stable solutions and they are, from a computational point of view, more efficient than the LEE, since they solve one equation less due to the fact that the isentropic relation between pressure and density is inherently satisfied. If only acoustic modes are excited by the source vectors and if the acoustic field can be assumed to be irrotational, LEE and APE render identical results.

DOI: 10.1002/fld

In order to investigate the effect of the mean flow field on the propagation of acoustic waves, different assumptions about the mean flow field are made. A first type of calculation is carried out with a mean flow field, obtained with a RANS calculation. The mean flow variables are then used for both LEE and APE. Another type of calculation is carried out using a uniform mean flow in the whole computational domain. For this latter type of flow field, the propagation equations (10)–(12) or (13)–(14) can be further simplified to the CWE:

$$\frac{\mathrm{D}^2}{\mathrm{D}t^2}p' - c_0^2\nabla^2 p' = \Phi_{\mathrm{ac}} \tag{15}$$

where $\mathrm{D}/\mathrm{D}t = (\partial/\partial t + \overrightarrow{U_0}\cdot\nabla)$ is the total time derivative. Comparing the results obtained with the CWE with those obtained with the APE gives an indication of the importance of non-uniform mean flow effects such as refraction. The influence of the mean flow convection effects is investigated by assuming a uniform medium at rest. In the latter case, the CWE can be further simplified in the form of the well-known linear AWE:

$$\frac{1}{c_0^2}\frac{\partial^2 p'}{\partial t^2} - \nabla^2 p' = \Phi_{\mathrm{ac}} \tag{16}$$

5.2. Coupling techniques

There are two major techniques to couple the source region with the acoustical domain: techniques using equivalent aeroacoustic sources, also referred to as acoustic analogies, and those using acoustic boundary conditions, which can be seen as an extension of Kirchhoff's method [11, 12].

5.2.1. Acoustic analogies. Lighthill [8] introduced the use of acoustic analogies. By rewriting the Navier–Stokes equations in such a way that the left-hand side equals the AWE (16) and taking the density as the acoustic variable, whereas all other terms are treated as right-hand side source terms, he obtained, for subsonic, isentropic flows, the following equation:

$$\frac{\partial^2 \rho}{\partial t^2} - c_0^2\nabla^2\rho = \frac{\partial^2 T_{ij}}{\partial x_i \partial x_j} \tag{17}$$

where T_{ij} is the Lighthill stress tensor defined as

$$T_{ij} = \rho u_i u_j + (p - c_0^2\rho)\delta_{ij} - \tau_{ij} \tag{18}$$

The approach of replacing the whole noise-generating flow field by an equivalent source term is appealing due to its simplicity and can be used to identify possible aeroacoustic source phenomena. Furthermore, these methods require less accurate source calculations, since they are based on aerodynamic fluctuations, and results obtained by incompressible computations or RANS calculations, when the turbulent field is stochastically reconstructed, can be used [6].

If a similar approach is used for rewriting the LEE, there would be only a contribution of the non-linear terms of the decomposed Navier–Stokes equations in the source term formulation. These terms are for most applications even neglected in the Lighthill stress tensor (18) and thus cannot be seen as an accurate representation of the true source-generating mechanism.

Ideally, the decomposition of the Navier–Stokes equation should be carried out with two fluctuating variables instead of one variable: an acoustic fluctuating part ($\rho'_{\mathrm{ac}}, u'_{\mathrm{ac}}, p'_{\mathrm{ac}}$) and an aerodynamic, or turbulent, fluctuating part ($\rho'_{\mathrm{t}}, u'_{\mathrm{t}}, p'_{\mathrm{t}}$). The latter fluctuating aerodynamic variables can

DOI: 10.1002/fld

be considered to be obtained from the flow domain calculation and are thus no unknowns for the LEE, which need to be solved for the acoustic fluctuating part. For such decomposition all terms containing the turbulent fluctuating variables should be treated as source terms, while the terms containing the acoustic fluctuating part should remain in the left-hand side [32, 33].

Nevertheless, in a large number of aeroacoustic applications, the turbulent variables in the source region are orders of magnitude larger than the acoustic variables, which reduces the necessity of such a decomposition. This results, for low Mach number and isentropic applications, in a source term contribution only in the momentum equations:

$$\Phi_{\text{mom},i} = -\frac{\partial}{\partial x_j}\rho_0(u_i u_j)' \tag{19}$$

This source term is identical to the source term proposed by Lighthill. It should be noted that for incompressible source region calculations or for sound generation by purely aerodynamic phenomena, where no flow-acoustic feedback is present, the fluctuating part contains no or a minor acoustic part and can thus be seen as an accurate source term definition. Since for the application of cavity noise the acoustic fluctuating part cannot be neglected if the cavity oscillates in shear-layer mode, it can be expected that the Lighthill tensor is not the most accurate source representation, since it contains a significant contribution $(\rho_0 U_{i0} u'_{j,\text{ac}} + \rho_0 u'_{i,\text{ac}} U_{j0})$ from the acoustic field.

For applications in which the acoustic field cannot be neglected, an aerodynamic/acoustic splitting procedure [33] or an alternative source term formulation is required. A possible alternative is proposed by Powell [34]. He proposed to consider only the rotational part of the flow variables as a source of sound. Since for most applications the acoustic variables can be assumed to be irrotational, the rotational fluctuating part can be considered as purely turbulent. The source term in the momentum equations, for a low Mach number isentropic flow, can then be expressed as

$$\Phi_{\text{mom},i} = -\rho_0(\boldsymbol{\omega}\times\mathbf{u})'_i = -\rho_0\mathbf{L}'_i \tag{20}$$

The major vortex source term is thus the fluctuating Lamb vector $\mathbf{L}'_i$. The same source term, divided by the mean density, is obtained when the Navier–Stokes equations are rewritten in such way that the left-hand side equals the APE [7]. For applications where the acoustic variables inside the source region are of the same order of magnitude as the turbulent variables, there might still be some influence $(\boldsymbol{\omega}_0\times\mathbf{u}_{\text{ac}})'_i$ of the acoustic fluctuations inside the source term if the mean flow is not irrotational.

Another type of acoustic analogy, studied in this paper, is proposed by Curle [9]. To take into account the influence of solid walls on the aerodynamically generated acoustic field, Curle suggested using the fluctuating aerodynamic forces, generated by the flow field, normal to the walls as the major source of aeroacoustic noise. These forces behave like an acoustic dipole with, for low Mach number applications, a much greater radiation efficiency than the quadrupole-like Lighthill sources, which can thus be neglected. For the LEE and APE, the fluctuating wall forces appear in the right-hand side of the momentum equations resulting in the following source terms, when the viscous forces near the walls are neglected:

$$\Phi_{\text{mom},i} = \int p'\,\mathrm{d}S_i \tag{21}$$

where S_i is the normal wall vector. Since the fluctuating forces at the wall can be considered to be entirely generated by the turbulent flow field, this type of source term formulation can be

DOI: 10.1002/fld

considered to be accurate, even when acoustic variables are of the same order of magnitude as the turbulent fluctuations, although they are very sensitive to the flow domain modeling near the walls.

In this paper, Lighthill source terms (19), vorticity source terms (20), and wall forces (21), calculated in the whole source region, are used as equivalent source term formulations. Toward the boundaries of the source region, the source terms are gradually damped toward zero. If the source terms are not smoothly damped out near the borders, they may create discontinuities, which may result in the generation of spurious acoustic waves. Furthermore, it avoids an artificial breakup of vortices traveling through the outflow boundary of the source region, which may result in a spurious contribution in the source term formulations. This is most apparent in the acoustic results in the downstream region if no artificial damping is applied.

5.2.2. Acoustic boundary conditions. Another way of coupling the results from the source region with the acoustic propagation equations is through the use of the fluctuating density, pressure, and velocity field as acoustic boundary conditions for the propagation equations. In this case, no additional source terms are required. This, however, imposes strong restrictions to the calculation of the source region. Commercial Computational Fluid Dynamics (CFD) codes, offering LES solution schemes, calculate the flow field with lower-order fairly dissipative numerical schemes without avoiding spurious reflections at the boundaries. If not taken care of properly, these numerical schemes and boundary conditions can introduce numerical noise inside the computational domain. These errors can become of the same order of magnitude as the acoustic variables needed for this type of coupling [35]. All these elements make the method of acoustic boundary conditions much more sensitive to the accuracy of the source region modeling as compared with the acoustic analogy approach. Furthermore, a compressible simulation is indispensable to capture any acoustic fluctuation, which is a serious computational disadvantage for low Mach number applications.

A problem that arises with the use of acoustic boundary conditions is that the surface on which the variables are calculated (the Kirchhoff surface) should be located far enough from the aeroacoustic sources and no turbulent flow should pass the boundary. If outflow occurs at the boundary, the velocity fluctuations may contain vorticity components, and density and pressure fluctuations may contain hydrodynamic and entropy fluctuations, which may excite the vorticity and entropy modes of the propagation equations. Near the Kirchhoff surface small instabilities may occur due to the fact that the fluctuating variables do not perfectly satisfy the propagation equations. For this reason artificial selective damping [36] is absolutely necessary. Especially, the APE can suffer from unstable solutions near the Kirchhoff surface when a turbulent flow passes this boundary since the presence of vorticity waves is not supported by the propagation equations.

A way of avoiding these problems is to carry out a filtering of the variables at the Kirchhoff surface in such a way that only purely acoustic fluctuations are used as boundary conditions. Ovenden and Rienstra [37] recently developed a method to match the flow variables with the acoustic modes of a slowly varying duct. In this way, only acoustic variables are taken into account in the propagation equations. An aerodynamic/acoustic filtering procedure [33] allows one to obtain the acoustic variables for non-ducted applications with strong vortical outflow.

A major advantage of the use of acoustic boundary conditions is that, when the boundary variables only contain acoustic fluctuations, this method can be seen as an acoustic continuation of the LES in the regions where no further noise sources are present [38]. In this way, if the flow domain calculation is accurate, it can be assumed that this coupling methodology renders the most accurate results. For this reason, the results obtained with acoustic boundary conditions are

DOI: 10.1002/fld

used as reference values in the remaining part of this paper. Comparison with the DNS results obtained by Rowley [1] confirms these findings. Another advantage of using acoustic boundary conditions is the fact that the propagation region does not contain the source region (white region in Figure 2) and thus a smaller propagation region needs to be considered as compared with the acoustic analogy approach.

In this paper, acoustic boundary conditions using the fluctuating pressure, density, and velocity components obtained with LES are used on a surface surrounding the source region. Owing to the use of a seven-point stencil finite-difference implementation of the acoustic propagation equations, the acoustic pressure surface has a thickness of three points. In this way, additional information about the directivity of the acoustic waves, propagating through the acoustic boundaries, is taken into account.

5.3. Numerical implementation

The propagation equations are discretized with a finite-difference method. The space derivatives are calculated with the fourth-order (seven-point stencil) dispersion-relation-preserving scheme [39]. In order to filter out spurious high-frequency grid-to-grid oscillations, artificial selective damping is added to the equations [36]. Time advancing is carried out with the five-stage low dispersion–dissipation Runge–Kutta scheme of Hu *et al.* [40]. It was shown in the previous research [41] that a combination of these numerical schemes provides, for CAA applications, an optimal compromise between high accuracy, low dispersion and dissipation errors, and reasonable computational efforts.

Three different kinds of boundary conditions must be specified: wall boundary conditions at the cavity walls, radiation boundary conditions at the inflow and top boundaries, and outflow boundary conditions at the outflow regions, where vorticity waves leave the computational domain. The radiation (for acoustic waves that leave the computational domain) and the outflow boundary conditions (for acoustic, vorticity, and entropy waves that leave the computational domain), derived by Tam and Dong [26] as an asymptotic solution of the LEE, are used. At outflow boundaries, similar as for the unsteady flow simulation, a buffer zone, containing 50 cells, is added to enhance the non-reflecting performance of this type of boundary conditions. At the walls, wall boundary conditions using one ghost point are used as proposed by Tam and Dong [42].

6. ACOUSTIC RESULTS

For the investigation of the influence of the coupling techniques, three types of equivalent aeroacoustic source term formulations—Lighthill sources, vorticity-based source terms, and fluctuating wall forces—are compared with the results obtained from the acoustic boundary conditions, which are referred to as the reference solution, since, as concluded in the previous section, they can be regarded as an acoustic continuation of the source domain simulation. For this study both LEE and APE are used, whereby the mean field outside the source region is obtained using a RANS calculation.

The study of the propagation equations uses both APE and LEE, taking into account all convection and refraction effects of the mean flow field onto the acoustic propagation. A next simulation uses the APE, where a uniform mean flow in the x-direction is imposed, resulting in a CWE formulation and thus neglecting any possible refraction effects. Finally, the APE are used for a medium at rest. This calculation is further referred to as the AWE, where no mean flow effects on

DOI: 10.1002/fld

the propagation of acoustic waves are taken into account. For all these simulations, the coupling is achieved using vorticity-based source terms.

The computational time necessary for all acoustic simulations is less than 5% of the computational time needed for the unsteady flow simulations. The total computational cost of the hybrid CAA methodologies is thus largely dominated by the cost of the flow simulations. Between the different acoustic simulations, the total CPU time obtained with the acoustic boundary conditions as the coupling technique is slightly lower due to the smaller computational domain. A detailed comparison between the total CPU times for the hybrid CAA simulations is, however, not included since the acoustic simulations using equivalent source term formulations can be possibly performed more efficiently, while maintaining a similar overall accuracy, using less accurate CFD simulations, such as incompressible simulations, traditional boundary conditions, etc. [38]. As already mentioned before, these simplifications of the unsteady flow simulations cannot be used when using acoustic boundary conditions.

6.1. Acoustic boundary condition results

6.1.1. Wake mode. The left side of Figure 8 shows the instantaneous pressure contours obtained with the LEE coupled through acoustic boundary conditions with the source region for the cavity oscillating in wake mode ($4M5$). The pressure contours show an acoustic propagation with a dominant radiation upstream of the cavity. Since the LEE support the propagation of vorticity waves, hydrodynamic pressure fluctuations are observed in the outflow region near the walls. When using the APE as propagation equations, these pressure fluctuations are not supported, which leads to instabilities in the final solution since the hydrodynamic fluctuations are inherently present in the boundary condition values. In the pressure spectrum at a point with coordinates $(-10.0D, 20.0D)$, shown on the right side of Figure 8, typical tonal peaks appear at the vortex shedding frequency ($St_D = 0.064$) and its higher harmonics, with amplitudes gradually decaying with increasing frequency.

The directivity patterns at the first two resonance frequencies ($St_D = 0.064$ and 0.128) are shown in Figure 9 on a half circle with radius $15.0D$ and center at the cavity trailing edge. The first

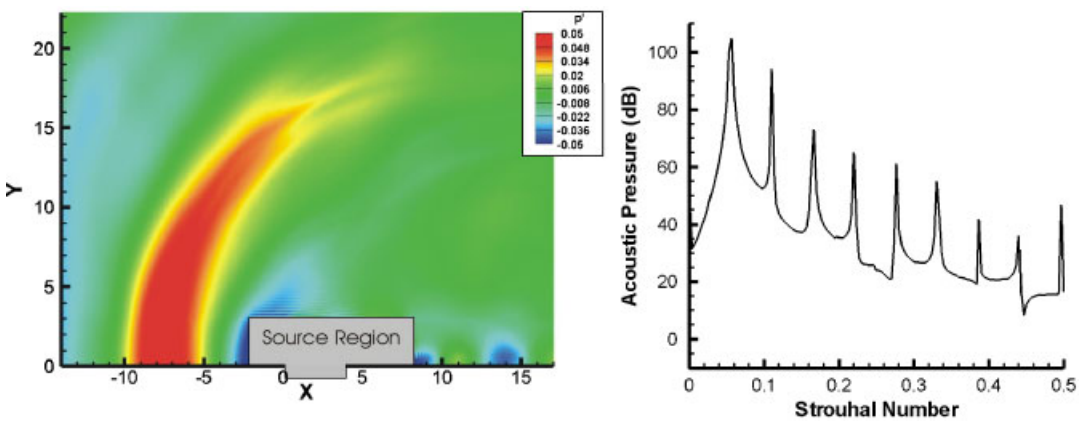

Figure 8. Instantaneous pressure contours (left) and pressure spectrum (dB) for the point $(-10.0D, 20.0D)$ (right) obtained with LEE and acoustic boundary conditions for the cavity $4M5$.

DOI: 10.1002/fld

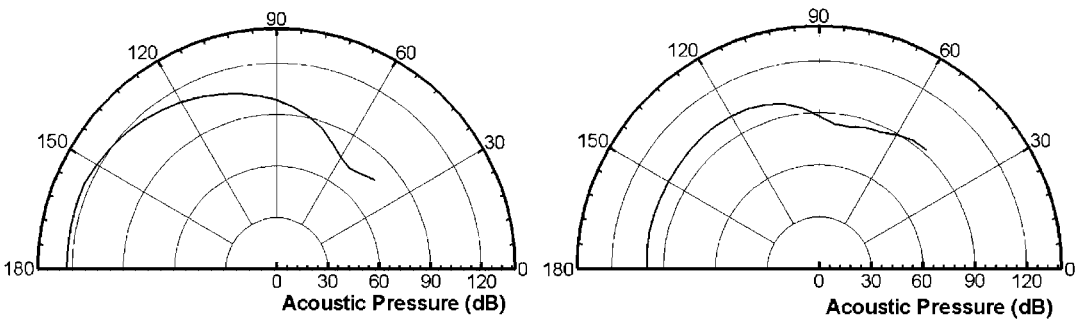

Figure 9. Directivity patterns of the pressure field (dB) at the first ($St_D = 0.064$, left) and second ($St_D = 0.128$, right) resonance frequencies obtained on a circle with radius $15.0D$ and center at the cavity trailing edge for the cavity $4M5$.

resonance shows a dominant propagation direction upstream of the cavity, with the maximal value near the upstream wall. The second resonance has a constant amplitude for angles above 90°. In the downstream direction (angles below 90°), the pressure decreases significantly, especially for the first resonance. At very small angles, the pressure is not shown, since pseudo-sound in these regions gives rise to high-amplitude aerodynamic pressure fluctuations, which cannot be considered as purely acoustical.

6.1.2. Shear-layer mode. The instantaneous pressure contours, shown on the left side of Figure 10, for the cavity $2M6$ oscillating in the shear-layer mode clearly evidence a different behavior as compared with the cavity $4M5$. A shorter acoustic wavelength and thus a higher resonance frequency is observed. Hydrodynamic pressure fluctuations near the downstream wall are still present but have a much lower amplitude, since the source region results show a much smaller perturbation of the boundary layer downstream of the cavity trailing edge. The pressure spectrum at the point $(-10.0D, 20.0D)$ is shown on the right side of Figure 10. The first Rossiter mode at $St_D = 0.19$ and its higher harmonics are present. The contribution of the higher harmonics of the resonance frequency is less pronounced as for the cavity $4M5$.

Directivity patterns at the first two resonance frequencies are shown in Figure 11. The first resonance shows a dominant propagation direction around 130°; at higher angles the pressure decreases again, opposite to the cavity $4M5$. This radiation pattern is identical to the prediction using an analytical Green's function [2]. The second resonance has a different radiation pattern. There is still a dominant propagation around 130° but also a downstream propagation at around 60° is observed, albeit with lower amplitude.

6.2. Effect of the source term formulation

6.2.1. Wake mode. The noise-generating mechanism for the cavity $4M5$ is a periodical vortex shedding at the leading edge of the cavity. The source region contains mostly turbulent fluctuations and the acoustic fluctuations are orders of magnitude smaller than these aerodynamic fluctuations. As a result, the different equivalent source term formulations contain primarily contributions from the turbulent field and only a minor, erroneous, contribution of the acoustic field inside the source region.

DOI: 10.1002/fld

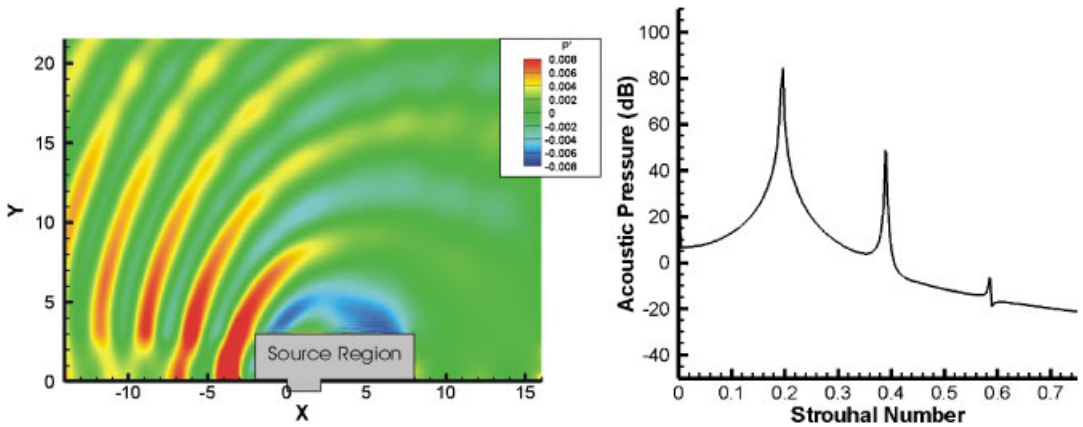

Figure 10. Instantaneous pressure contours (left) and pressure spectrum (dB) for the point $(-10.0D, 20.0D)$ (right) obtained with LEE and acoustic boundary conditions for the cavity $2M6$.

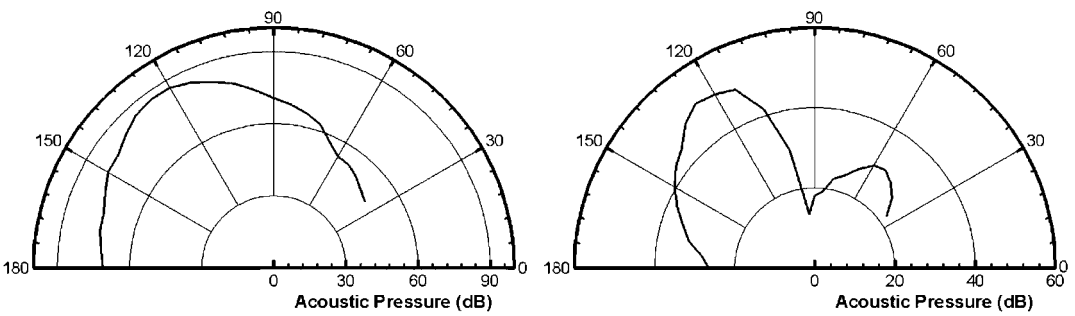

Figure 11. Directivity patterns of the pressure (dB) at the first ($St_D = 0.19$, left) and second ($St_D = 0.38$, right) resonance frequencies obtained on a circle with radius $15.0D$ and center at the cavity trailing edge for the cavity $2M6$.

The results, obtained with the LEE, coupled with different aeroacoustic source term formulations are shown in Figure 12 and are in good agreement with the results obtained with the acoustic boundary conditions. Both the pressure spectrum and the directivity pattern are accurately predicted, although it can be noticed that the amplitude at the higher harmonics of the vortex shedding frequency is overpredicted for all equivalent source term formulations. The directivity pattern at higher angles is similar to that obtained with the acoustic boundary conditions. In the downstream direction, an overestimation is noticed. This overestimation, caused by the use of the LEE, is discussed in more detail in the following section. The results obtained with Curle's analogy underestimate the sound pressure levels at higher frequencies due to the fact that the Van Driest wall damping damps out pressure fluctuations near the walls, resulting in lower wall forces and thus lower source term contributions [38].

6.2.2. Shear-layer mode. As already mentioned before, the noise-generating mechanism for the cavity $2M6$ is significantly different from that of the cavity $4M5$. The turbulent velocity fluctuations

DOI: 10.1002/fld

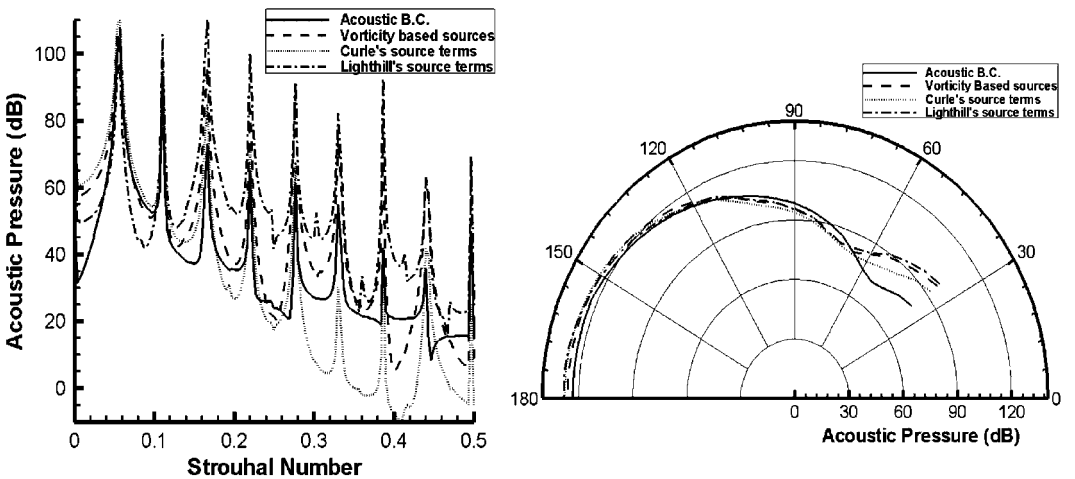

Figure 12. Pressure spectrum (dB) for the point $(-10.0D, 20.0D)$ (left) and directivity pattern of the pressure field (dB) at $St_D = 0.064$ on a circle with radius $15.0D$ and center at the cavity trailing edge (right) for the cavity $4M5$ obtained with different source term formulations (solid: acoustic B.C., dashed: vorticity-based source terms, dotted: fluctuating wall forces, dash-dotted: Lighthill sources).

are much smaller and acoustic fluctuations are of the same order of magnitude. This leads to a large contribution of acoustic variables inside the source term formulations, resulting in an overestimation of the source term contributions and the subsequent sound pressure levels, as illustrated on the left side of Figure 13. The overprediction is more apparent for Lighthill's source terms since they are more sensible to these errors, as explained in the previous sections. The underestimation of the sound pressure levels with Curle's analogy is similar as for the cavity oscillating in wake mode, caused by the Van Driest damping near the walls.

Next to the overestimation of the sound pressure levels, the directivity pattern at the first Rossiter mode, shown on the right side of Figure 13, is inaccurately predicted. The dominant propagation direction is shifted downstream for both the vorticity-based and Lighthill's source terms, resulting in a different radiation pattern. The downstream shift in the radiation direction is caused by the erroneous contribution of the acoustic fluctuations in the source term formulations. In this way, acoustic convection effects are introduced in the equivalent sources of the LEE, which counteract with the convection effects that are introduced by the propagation equations. As a result, the convective effects are underestimated in the resulting acoustic field.

Curle's analogy is clearly more able to predict the right propagation direction, although, in this case, a slight shift toward the upstream direction is observed. This is caused by inaccuracies of the LES simulation in the vicinity of the walls. Since Curle's analogy only uses fluctuating aerodynamic values at the walls, the final acoustic results are very sensitive to the accuracy of the near wall results of the source region simulation.

6.3. Effect of the propagation equations

For the cavity $4M5$, a significant difference between the APE and LEE is only apparent in the downstream direction, as shown in Figure 14. This is caused by the fact that the rotational component of the flow field, which is only modeled in the LEE, has a significant influence on

DOI: 10.1002/fld

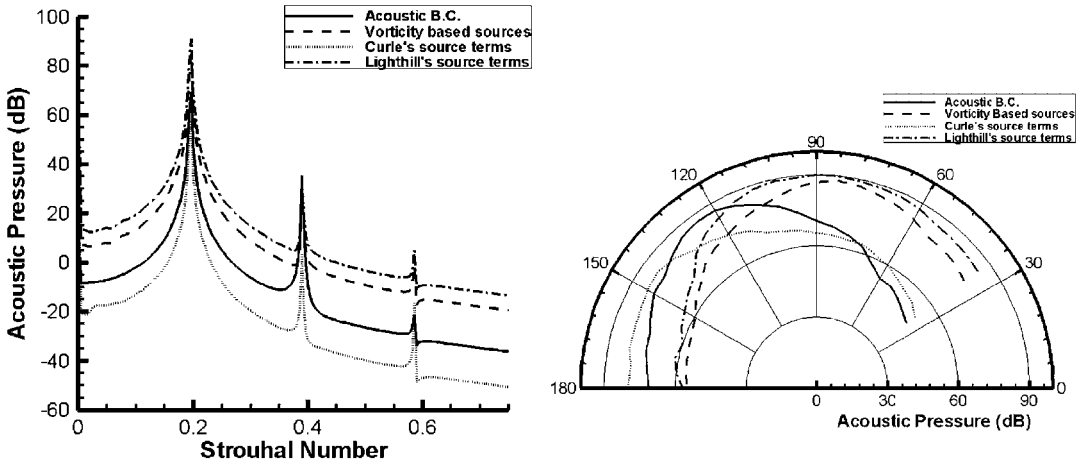

Figure 13. Pressure spectrum (dB) for the point $(-10.0D, 20.0D)$ (left) and directivity pattern of the pressure field (dB) at $St_D = 0.19$ on a circle with radius $15.0D$ and center at the cavity trailing edge (right) for the cavity $2M6$ obtained with different source term formulations (solid: acoustic B.C., dashed: vorticity-based source terms, dotted: fluctuating wall forces, dash-dotted: Lighthill sources).

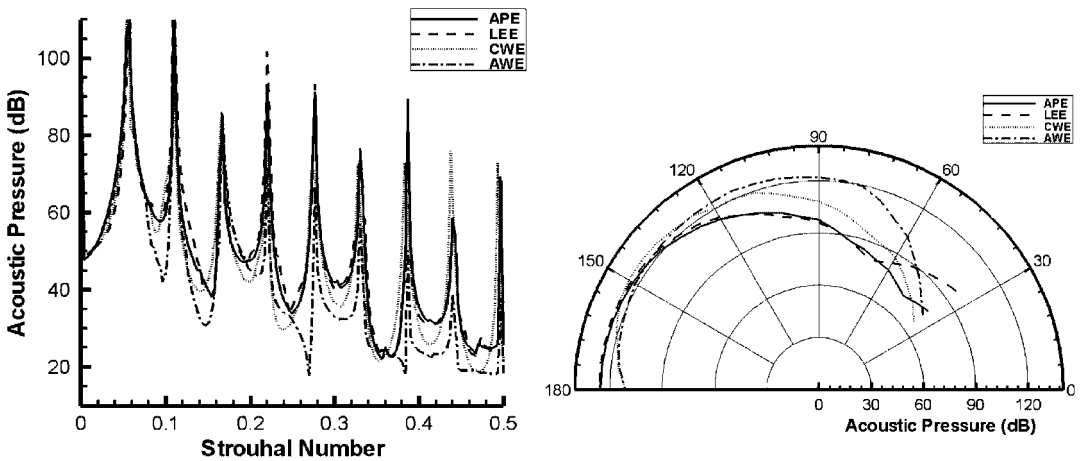

Figure 14. Pressure spectrum (dB) for the point $(-10.0D, 20.0D)$ (left) and directivity pattern of the pressure field (dB) at $St_D = 0.064$ on a circle with radius $15.0D$ and center at the cavity trailing edge (right) for the cavity $4M5$ obtained with different propagation equations (solid: APE, dashed: LEE, dotted: CWE, dash-dotted: AWE).

the downstream region and causes an additional, spurious, contribution to the acoustic field. In the upstream region, where the flow field can be assumed to be irrotational, there is only a minor contribution from the rotational part and thus no significant difference between LEE and APE is noticed. In general, the APE results are in better agreement with the results obtained with coupling through acoustic boundary conditions.

DOI: 10.1002/fld

The effect of the mean flow gradients, causing refraction of the acoustic waves, is evaluated by comparing the results obtained with the APE and the LEE with a non-uniform mean flow with the results obtained by using the APE with a constant, uniform mean flow (CWE). The directivity pattern is only changed near the walls, where the strongest mean flow gradients are present. The mean flow gradients inside the cavity have only a minor influence on the far-field radiation. Convection effects, on the other hand, clearly influence the far-field radiation. When assuming no mean flow (AWE), the directivity pattern is shifted toward the downstream direction, and sound pressure levels become slightly lower near the walls. This indicates that the presence of a mean flow is responsible for the dominant acoustic radiation in the upstream direction.

The mean flow effects for the cavity $2M6$ are more difficult to interpret, since mean flow effects can only be investigated by using acoustic analogies. When using acoustic boundary conditions as the coupling technique, these mean flow effects are inherently present in the boundary condition values. It has already been shown in the results of the cavity oscillating in the shear-layer mode that these calculations with a coupling based on an equivalent aeroacoustic source term formulation yield an erroneous propagation direction and thus make a comparison between the different propagation equations unreliable. For this reason, the previous analysis is not carried out for the cavity $2M6$ although it can be expected that similar conclusions as for the cavity $4M5$ hold.

7. CONCLUSIONS

In this paper, LES are successfully applied to the identification of the two flow-induced oscillation regimes that may occur in 2D rectangular cavities at low Reynolds number. The computations reveal the characteristic features of these two regimes. The shear-layer or Rosssiter mode is characterized by a flow-acoustic feedback coupling where the main oscillation frequencies are related to the Mach number. In the wake mode regime, the frequencies of oscillation are independent of Mach number and the incoming boundary layer is clearly affected by the oscillation pattern. From the quantitative point of view, good agreement has been found with the results reported by other authors.

Acoustic far-field results are obtained with a hybrid CAA methodology, where the LES results are coupled with different types of propagation equations. LEE and an irrotational formulation of the LEE, the APE, are used as propagation equations. It is shown that both sets of equations obtain similar results in the upstream direction. In the outflow region, rotational components, generated by vorticity waves in the source region, cause an overestimation of the sound pressure level and an overprediction of the radiation in the downstream region. By comparing the results obtained with different mean field assumptions, it is clear that refraction, generated by the mean flow gradients, causes an amplification of the sound pressure levels in the vicinity of the upstream wall. Convection effects result in a convective amplification and a shift of the dominant acoustic radiation in the upstream direction.

Two different coupling strategies have been adopted. The first uses velocity, density, and pressure fluctuations on a surface, immersed in the LES domain, as boundary conditions for the propagation equations. This technique can be seen as an acoustic continuation of the source region calculation. The results obtained with this coupling procedure are, for both cavities, in good agreement with the results reported by other authors, making this approach the most accurate coupling technique. This coupling strategy requires accurate source region results and can only be used with compressible source region calculations where special care is taken regarding the non-reflectiveness of the

DOI: 10.1002/fld

boundary conditions. It is shown that this type of coupling technique can only be used with the LEE since vorticity and entropy waves are present in the boundary values and are not supported by the APE, which can result in instabilities. If vortical outflow through the coupling surface is occurring, hydrodynamic pressure fluctuations are noticed in the vicinity of the downstream walls. In order to obtain accurate acoustic results in the downstream region, filtering of the coupling surface values is needed for this type of coupling technique.

The other coupling approach that is reported in this paper consists of replacing the whole source region by equivalent aeroacoustic source terms. Three types of aeroacoustic analogies are compared: Lighthill's source terms, vorticity-based source terms, and source terms based on the fluctuating wall forces. For the cavity oscillating in the wake mode, the fluctuating terms inside the source region contain a negligible amount of acoustic fluctuations and can be considered as purely turbulent. This leads to an accurate prediction of the sound pressure levels and the radiation pattern. Both Lighthill's source terms and vorticity-based source terms slightly overestimate the amplitude of the higher harmonics of the vortex shedding frequency. The dissipation, introduced by the Van Driest wall damping in the LES calculation, causes an underestimation of the wall forces, which results, at higher frequencies, in lower sound pressure levels, when Curle's analogy is used.

It is shown that, if acoustic fluctuations inside the source region are of the same order of magnitude as the turbulent fluctuations, special care is needed when using equivalent aeroacoustic source formulations. The source terms may contain a significant contribution from the acoustic field, resulting in an erroneous prediction of the acoustic far-field. For the cavity oscillating in the shear-layer mode, it is noticed that both the sound pressure levels and the radiation pattern are not predicted with sufficient accuracy, when using an equivalent source term formulation. It is noticed that vorticity-based source terms suffer less from these errors compared with a Lighthill type of source term formulation. In order to be able to produce accurate source terms for applications where the acoustic fluctuations inside the source region are not negligible, a distinction between a fluctuating acoustic field and a fluctuating turbulent, or noise-generating, field is needed, which is the case e.g. for the cavity oscillating in the shear-layer mode or for in-duct aeroacoustic applications.

It can be expected that the same conclusions hold for other cavity simulations with different Mach or Reynolds numbers. It should be mentioned that the wake mode, obtained for the simulation of the cavity $4M5$, is generally not observed for 3D simulations, where only the shear-layer mode can be identified. Special care is thus needed for the accurate modeling of the mutual interaction between the acoustic and aerodynamic fields when performing 3D simulation. If not taken care of properly, hybrid CAA simulation can, similar as for the presented 2D results, lead to inaccurate predictions of the acoustic near- and far-field radiation.

ACKNOWLEDGEMENTS

The authors want to acknowledge the financial support given by the Research Foundation of Flanders (FWO G.0467.05) and the Institute for the Promotion of Innovation by Science and Technology in Flanders (SBO-IWT 05.0163).

REFERENCES

1. Rowley CW. Modeling, simulation and control of cavity flow oscillations. *Ph.D. Dissertation*, California Institute of Technology, Pasadena, CA, 2002.

DOI: 10.1002/fld

2. Groerfelt X. Bruit Rayonne par un Ecoulement Affleurant une Cavite: simulation Aeroacoustique Directe et Application de Methodes Integrales. *Ph.D. Dissertation*, Laboratoire de Mcanique des Fluides et dAeroacoustique, cole Centrale de Lyon, France, 2001.
3. Shieh CM, Morris PJ. Parallel numerical simulation of subsonic cavity noise. *AIAA Paper 99-1891*, 1999.
4. Ricot D, Maillard V, Bailly C. Numerical simulation of the unsteady flow past a cavity and application to sunroof buffeting. *AIAA Paper 2001-2112*, 2001.
5. Gloerfelt X, Bogey C, Bailly C. LES of the noise radiated by a flow over a rectangular cavity. *Proceedings of the LES for Acoustics*, *DGLR Report 2002-03*, Gottingen, Germany, 2002.
6. Bailly C, Juv D. Numerical solution of acoustic propagation problems using linearized Euler equations. *AIAA Journal* 2000; **38**:22–29.
7. Ewert R, Schroder W. Acoustic perturbation equations based on flow decompositon via source filtering. *Journal of Computational Physics* 2003; **188**:365–398.
8. Lighthill MJ. On sound generated aerodynamically. I. General theory. *Proceedings of the Royal Society of London* 1952; **A211**(1107):564–587.
9. Curle N. The influence of solid boundaries upon aerodynamic sound. *Proceedings of the Royal Society of London* 1955; **A231**:505–514.
10. Ffowcs Williams JE, Hawkings DL. Sound generation by turbulence and surfaces in arbitrary motion. *Philosophical Transactions of the Royal Society* 1969; **A264**(1151):321–342.
11. Lyrintzis AS. The use of Kirchhoff's method in computational aeroacoustics. *Journal of Fluids Engineering* 1994; **116**:665–676.
12. Lyrintzis AS. Surface integral methods in computational aeroacoustics—from the (CFD) near-field to the (acoustic) far-field. *International Journal of Aeroacoustics* 2003; **2**:95–128.
13. Ahuja KK, Mendoza J. Effects of cavity dimensions, boundary layer and temperature on cavity noise with emphasis on benchmark data to validate computational aeroacoustic codes. *Technical Report 4653*, NASA CR, 1964.
14. Rossiter JE. Wind tunnel experiments on the flow over rectangular cavities at subsonic and transonic speeds. *Royal Aircraft Establishment Technical Report 64037*, 1964.
15. Gharib M, Roshko A. The effect of flow oscillations and cavity drag. *Journal of Fluid Mechanics* 1987; **177**:501–530.
16. Heller HH, Blis DB. Aerodynamically induced pressure oscillations in cavities: physical mechanisms and suppression concepts. *AFFDL Technical Report 74-133*, 1975.
17. Rockwell D, Naudascher E. Review: self-sustained oscillations of flow past cavities. *Journal of Fluids Engineering* 1978; **100**:477–506.
18. Komerath NM, Ahuja KK, Chambers FW. Prediction and measurement of flows over cavities—a survey. *AIAA Paper 82-022*, 1987.
19. Grace SM. An overview of computational aeroacoustics techniques applied to cavity noise prediction. *AIAA Paper 2001-0510*, 2001.
20. Larsson J, Davidson L, Olsson M, Eriksson LE. Aeroacoustic investigation of an open cavity at low Mach number. *AIAA Journal* 2004; **42**:2462–2473.
21. Guilloud G, Martinez-Lera P, Zacharopoulos C, Schram C. Optimization of hybrid aeroacoustic computations of an industrial confined flow through mesh coarsening techniques. *Proceedings of the International Conference on Sound and Vibration*, *ISMA 2008*, Leuven, Belgium, 2008; 471–484.
22. Vreman B. Direct and large eddy simulation of the compressible turbulent mixing layer. *Ph.D. Dissertation*, Department of Applied Mathematics, University of Twente, Enschede, The Netherlands, 1995.
23. Deardorff JW. A numerical study of three-dimensional channel flow at large Reynolds numbers. *Journal of Fluid Mechanics* 1970; **41**(2):453–480.
24. Kim JW, Lee DJ. Generalized characteristic boundary conditions for computational aeroacoustics. *AIAA Journal* 2000; **38**:2040–2049.
25. Poinsot TJ, Lele SK. Boundary conditions for direct simulations of compressible viscous flow. *Journal of Computational Physics* 1992; **101**:104–129.
26. Tam CKW, Dong Z. Radiation and outflow boundary conditions for direct computation of acoustic and flow disturbances in a nonuniform mean flow. *Journal of Computational Acoustics* 1996; **4**:175–201.
27. Collonius T, Lele SK, Moin P. Boundary conditions for direct computations of aerodynamic sound. *AIAA Journal* 1993; **31**:1574–1582.

DOI: 10.1002/fld

28. Rubio G, De Roeck W, Meyers J, Baelmans M, Desmet W. Numerical identification of flow-induced oscillation modes in rectangular cavities using large eddy simulations. *International Journal for Numerical Methods in Fluids* 2007; **53**:851–866.
29. Rubio G. Numerical methodologies for the determination of noise sources in subsonic flows. *Ph.D. Thesis*, K.U. Leuven, Belgium, 2007.
30. Seo JH, Moon YJ. Perturbed compressible equations for aeroacoustic noise prediction at low Mach numbers. *AIAA Journal* 2005; **43**:1716–1724.
31. Seo JH, Moon YJ. Linearized perturbed compressible equations for aeroacoustic noise prediction at low Mach numbers. *Journal of Computational Physics* 2006; **218**:702–719.
32. Chu B-T, Kovásznay B-T. Non-linear interactions in a viscous heat conducting compressible gas. *Journal of Fluid Mechanics* 1958; **3**:494–514.
33. De Roeck W, Baelmans M, Desmet W. Aerodynamic/acoustic splitting technique for computation aeroacoustics applications at low-Mach numbers. *AIAA Journal* 2008; **46**:463–475.
34. Powell A. Theory of vortex sound. *Journal of the Acoustical Society of America* 1964; **36**:177–195.
35. Tam CKW. Computational aeroacoustics: issues and methods. *AIAA Journal* 1995; **33**:1788–1796.
36. Tam CKW, Webb JC, Dong Z. A study of the short wave components in computational acoustics. *Journal of Computational Acoustics* 1993; **1**:1–30.
37. Ovenden NC, Rienstra S. Mode-matching stategies in slowly varying engine ducts. *AIAA Journal* 2004; **42**: 1832–1840.
38. De Roeck W, Rubio G, Baelmans M, Sas P, Desmet W. The influence of flow domain modelling on the accuracy of direct and hybrid aeroacoustic noise calculations. *AIAA Paper 2006-2419*, 2006.
39. Tam CKW, Webb JC. Dispersion-relation-preserving schemes for computational aeroacoustics. *Journal of Computational Physics* 1993; **107**:262–281.
40. Hu FQ, Hussaine MY, Manthey JL. Low-dissipation and low dispersion Runge–Kutta schemes for computational aeroacoustics. *Journal of Computational Physics* 1996; **124**:177–191.
41. De Roeck W. Hybrid methodologies for the computational aeroacoustic analysis of confined subsonic flows. *Ph.D. Thesis*, K.U. Leuven, Belgium, 2008.
42. Tam CKW, Dong Z. Wall boundary conditions for high-order finite-difference schemes in computational aeroacoustics. *Theoretical and Computational Fluid Dynamics* 1994; **6**:303–322.

DOI: 10.1002/fld